Mechanics of Golf Club and Ball Materials

MSE 733: Advanced Mechanics of Deformation

Tarun Vabhav Pratap Sikri

April 17, 2018

Abstract

The golf swing is a complex motion that requires accuracies and precisions orders of magnitude greater than other ball sports. Thus, an improved understanding of club and ball material mechanics during the golf swing would assist the coach and athlete to select optimized equipment that would complement an individual's unique swing character. Additionally, this would allow R&A and USGA governing bodies to impose conformance criteria that encourage equipment innovations yet maintain the game primarily as a test of the athlete's skill and not technological superiority of the equipment.

Table of Contents

I. Introduction……..……..2

II. Inertia Tensor……..……...3

III. Club Geometry……..…….4

IV. Swing Mechanics……...…….5

V. Shaft Material Mechanics…….8

VI. Impact Geometry and Ball Flight……..…….10

VII. Clubhead Material Mechanics……12

VIII. Ball Material Mechanics……. ……15

IX. Impact Modeling……..16

X. Conclusion……17

References: APA Format……18

"Anyone who hopes to reduce putting or any other department of golf to an exact science is in for serious disappointment and will only suffer from the attempt. "

Robert Tyre (Bobby) Jones Jr.
ME, Georgia Tech, 1922
Professional Golfer

I. Introduction

Historians trace the origins of golf to a Roman game of *Pangania* in which participants utilized a bent stick to hit a stuffed leather ball. Accompanied by Roman conquests this pastime activity spread throughout Europe during the first century BC. The modern game of golf was developed in 15th century Scotland. The Old Course at Saint Andrews is considered the oldest continuously operating golf course in the world, it was pivotal to the development of the sport and how the game is played today. The Royal and Ancient Golf Club of Saint Andrews founded on May 14, 1754 came to be regarded as the primary governing authority for golf around the world. A major reorganization in 2004 devolved these responsibilities to the R&A and United States Golf Association (USGA). Working together these two organizations share a commitment to a single code for the rules of playing golf, rules of amateur status and equipment standards. Modern golf clubs and balls are far superior compared to their predecessors from hundreds of years ago thus enabling a skilled player to hit the ball greater distances (Fig 1) with greater control and accuracy. New golf club and ball designs require submission to the R&A and USGA for evaluation as conforming product. This ensures that the sport remains a test of the athlete's skill level and not technological superiority of the equipment used [1,2].

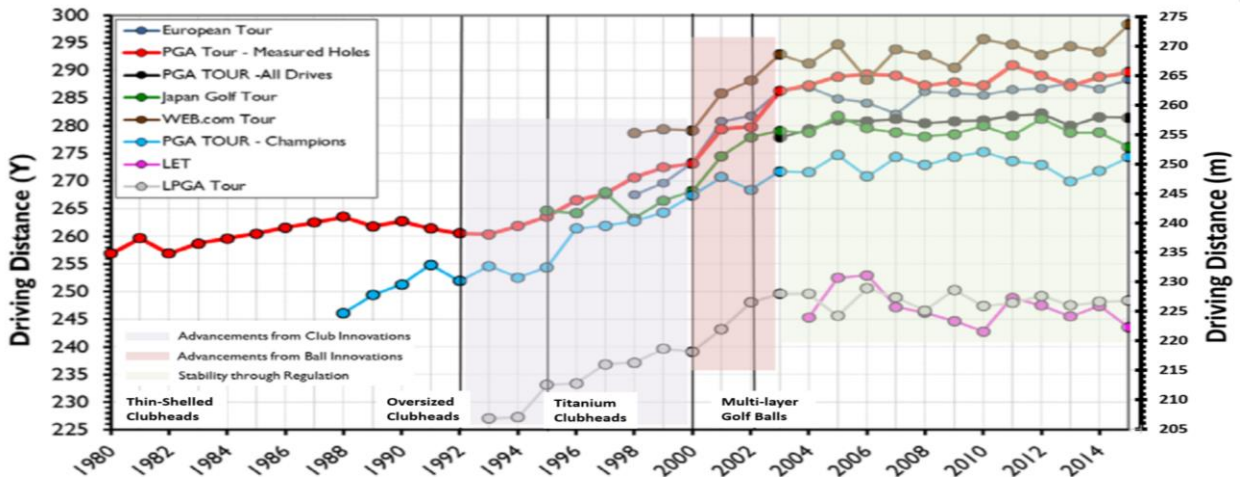

Figure 1: Average driving distances of major tours indicate distinct increases coincident with significant material advances [3].

The goal of the sport is to utilize external implements (golf clubs) of varying sizes and shapes to strike a ball into a series of 18 holes in as few strokes as possible. The playing area is non-standardized. Distances between the starting tee box and hole vary anywhere between 50 to 450 m, this involves varying terrains, water hazards, sand bunkers and grass types arranged into unique layouts. The required levels of precision and accuracy is orders of magnitude greater compared to any other ball sport. This challenges the athlete to create diverse types of shots depending on their self-confidence and skill level. Thus, an improved understanding of golf club and ball material mechanics would assist the athlete and coach to select optimum equipment based on individual swing characteristics [4].

II. Inertia Tensor

Mass distribution of a rigid body about its center of mass (CM) can be generalized by a 2nd rank, symmetric inertia tensor. Where m_i are discrete masses of the total mass M and x_i, y_i, z_i are

$$[I]_{CM} = \begin{bmatrix} \sum m_i(y_i^2 + z_i^2) & \sum m_i x_i y_i & \sum m_i x_i z_i \\ - & \sum m_i(x_i^2 + z_i^2) & \sum m_i y_i z_i \\ - & - & \sum m_i(x_i^2 + y_i^2) \end{bmatrix} \quad (1)$$

the corresponding cartesian coordinates. Characteristic eigenvalues of $[I]_{CM}$ allows determination of a principal inertia tensor through the CM.

$$[I]_P = \begin{bmatrix} I_{zz} & 0 & 0 \\ 0 & I_{zz} & 0 \\ 0 & 0 & I_{zz} \end{bmatrix} \quad (2)$$

The Parallel Axis Theorem is used to define an equivalent [I] about an arbitrary point S that is

$$[I]_A = [I]_{CM} + M[\vec{d}]^2 \quad (3)$$

separated $\vec{d}$ away from the CM. A rigid body with angular velocity $\vec{\omega}$ has angular momentum

$$\vec{L} = [I]_A \vec{\omega} \tag{4}$$

Torque is defined as the time derivative of angular momentum.

$$\vec{T} = \frac{d\vec{L}}{dt} \tag{5}$$

Kinetic energy is a scalar value defined as an inner product [5].

$$K = \frac{1}{2}\vec{\omega}^T [I]_A \vec{\omega} \tag{6}$$

These kinematic relations indicate that [I] directly correlates to a generalized resistance to rotation. Global X-Y-Z cartesian coordinates will be utilized to describe impact geometry and ball flight. Separate and local X-Y-Z cartesian coordinates will be utilized to describe downswing club motion, downswing shaft deflections and mass-inertial properties of the clubhead.

III. Club Geometry

During play a maximum of 14 clubs are allowed per golfer and no club adjustments are allowed. A typical assortment includes: 1 through 3 woods (drivers), 4 through 9 irons[1], pitching wedge, sand wedge, putter. Increasing club number corresponds to decreasing shaft lengths (1.14 – 0.91 m) and carry distances, increasing clubhead lofts (8 – 60^o) and clubhead masses (200 – 300 g). Woods (1 - 3) are utilized for long tee shots, mid-irons (4 - 9) are utilized for shorter tee and fairway shots. Short irons (pitching, sand wedge) are typically used for approach shots onto the green so that ball landing position and stopping distance near the hole can be better controlled. A putter is used once the ball arrives onto the green. The athlete grips the club on the larger diameter end of a hollow tapered shaft. The clubhead hosel is secured onto the smaller diameter end using either thermoset epoxy or a lock screw (Fig 2a). Parallel grooves inscribed onto the clubface deflect undesired impediments such as water, dirt, sand and grass away from the impact area improving

[1]The word “iron” used throughout this text refers to clubs numbered 4 through 9. The iron chemical species is referred by its elemental symbol (Fe).

clubface-ball friction during impact. Lie is the angle defined between the clubhead sole and shaft axis (Fig 2b), loft is the angle defined between the face normal and sole resting on a level surface (Fig 2b) [1,2]. Optimum lie and loft angles are fitted based upon a golfer's anatomical considerations. A static balance measurement of driver and iron clubs is utilized to quantify "feelings of heaviness" (swing-weight) for the golfer (Fig 2c). Designated by a Prorythmic Scale, letters A through D and numbers 0 through 10 correspond to increasing swing-weights. Determination of ideal swing-weights based upon a combined $[I]_A$ of the club and straight left forearm of the golfer relative to the left shoulder joint is an area of active research [6].

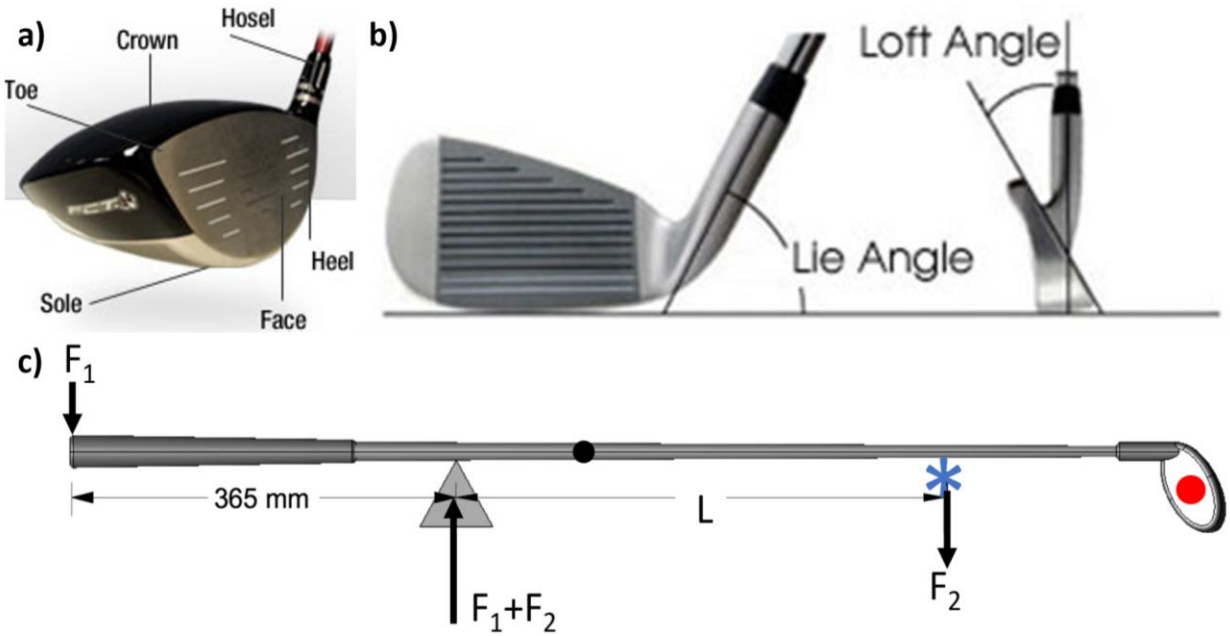

Figure 2: Regions of a clubhead geometry (a) include: toe, face, sole, crown, heel and hosel. Lie and loft (b) are defined as angles between the shaft axis and clubhead sole when viewed from the clubhead face and side views respectively [1,2]. Clubhead CM (red circle) and shaft CM (black circle) result in a total club CM (blue star) offset from the shaft axis (c). A static balance point measurement utilizes a fulcrum position on the shaft 365mm away from the grip end. Total club CM exerts a downward force (F_2), and the measured force (F_1) at the grip end corresponds to a swing-weight designation [6].

IV. Swing Mechanics

A golf swing is defined as a sequence of events that enables the athlete to hit the ball to a desired location, this involves: planning, address, backswing, transition, downswing, impact and follow-through. The planning stage involves club selection based on the desired aim direction,

distance, and external factors such as terrain and wind conditions. Address involves feet alignment relative to the ball position and target direction, hand placement on the club grip, and posture that biomechanically enables the body to fire in a sequential pattern. The backswing displaces the clubhead away from the ball and eccentrically stretches large skeletal muscles creating stored elastic potential energy. Ground reaction forces initiate transition from the backswing to downswing (Fig 3g), rapid concentric muscle contractions exert torques which release this stored potential into kinetic energies. Rapid deceleration of preceding body segments create opposing interactive torques at the connecting joints (Fig 3a), this ensures efficient kinetic energy transfer through the body to the clubhead. Passive torques applied at the wrist orient the club and forearm into specific positions resulting in efficient accelerations so that clubhead velocity is maximized upon impact (eq 1-3, Fig 3 b-e). The early downswing (Fig 3h) is characterized by a $|[I]\hat{\imath}|$ local minimum resulting in a $\vec{\omega}\hat{\imath}$ local maximum, this rotates the clubhead CM around the spinal axis (alpha rotation). The middle downswing (Fig 3i) is characterized by a $|[I]\hat{\jmath}|$ local minimum resulting in a $\vec{\omega}\hat{\jmath}$ local maximum, this rotates the clubhead CM above the hand path (beta rotation). Late downswing (Fig 3j) is characterized by a $\left|[I]\hat{k}\right|$ local minimum resulting in a $\vec{\omega}\hat{k}$ local maximum, this rotates the clubhead CM about the shaft axis closing the clubface (gamma rotation). Empirical data from professional golfers has validated these Double Pendulum, Inverse Dynamics and Forward Dynamics downswing models. Initial address position of the golfer (Fig 3f) defines the local static Cartesian Coordinate system with origin situated on the left shoulder; spinal axis, target line and shaft are coincident with the +x, +y and +z axes respectively [7, 8, 9, 10].

Shorter shafted, more lofted clubs necessitate a clubhead downswing path that is closer to perpendicular relative to the standing surface. This is promoted by an address position with a narrower stance and more anteriorly reclined posture. Longer shafted, less lofted clubs necessitate

a clubhead downswing path that is closer to parallel relative to the standing surface. This is promoted by an address position with a wider stance and more posteriorly reclined posture.

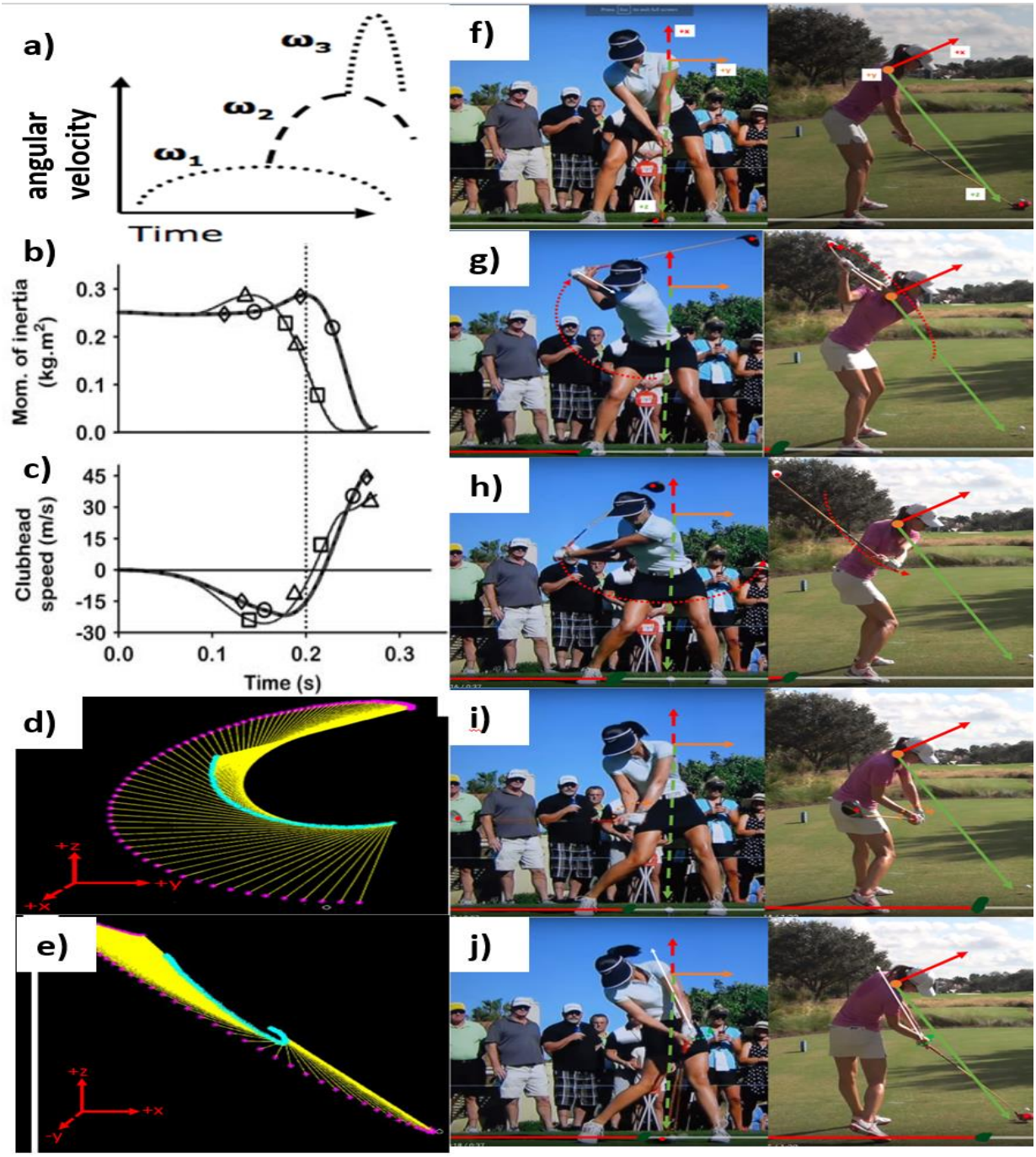

Figure 3: Rapid deceleration of larger, slower proximal links (a) result in efficient transfer of kinetic energies so that proximal (clubhead) speed can be maximized [7]. Computer simulations and empirical data validates the late downswing is characterized by a local $\left|[I]\hat{k}\right|$ minimum (b) resulting in rapid clubface closure (c) (gamma motion) [8]. Stroboscopic face-on (d) and target line views demonstrate clubhead (pink dots) and grip (blue dots) positions at regular time intervals, yellow lines represent the shaft axis. Face-on and target line views demonstrate address (f), backswing-downswing transition (g), early downswing (h), middle downswing (i) and impact (j) [9].

V. Shaft Material Mechanics

Greater tangential forces applied at the grip during the early and middle downswing deflect the clubhead CM toward the shaft CM, this is manifested as toe-up and lag deflections. Greater axial (centripetal) forces applied at the grip during the late downswing deflect the clubhead CM away from the shaft CM; this is manifested as toe-down and lead deflections. The position of maximum shaft curvature at impact (kick-point) results in a dynamic loft. The local shaft Cartesian Coordinate system is defined by the shaft (+z) axis at all times [10].

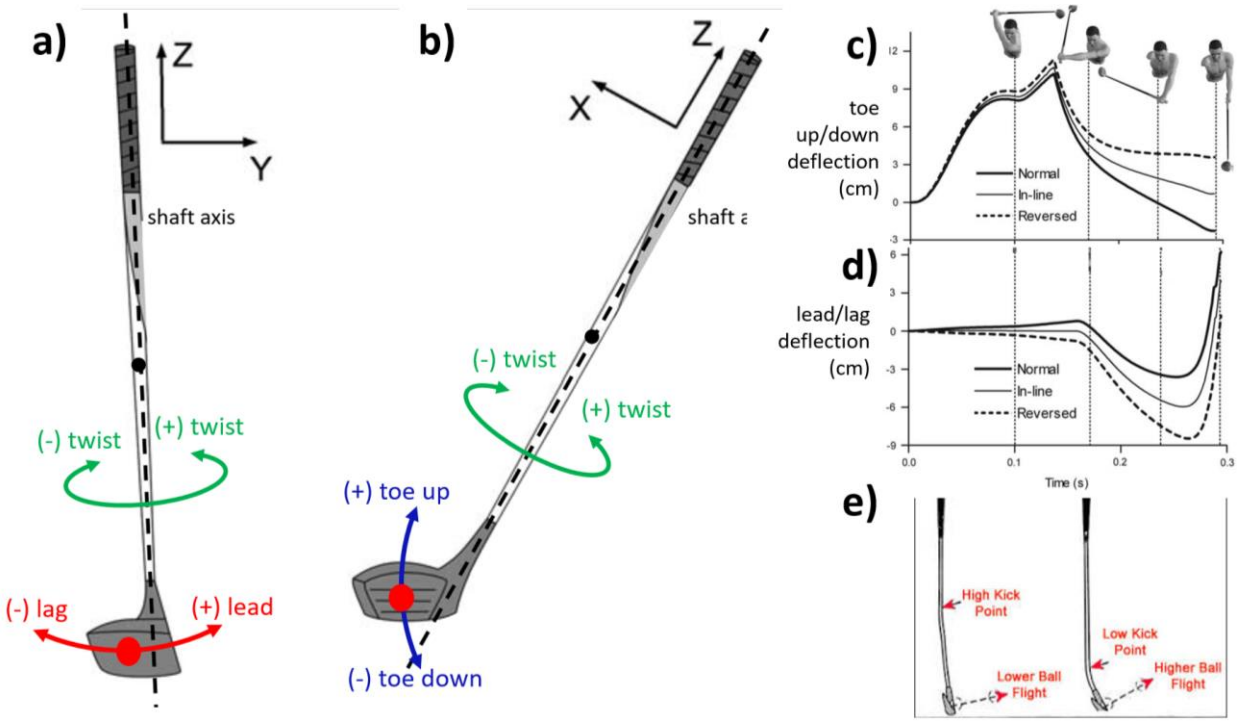

Figure 4: Clubhead CM (red circle) is offset from the shaft axis, and thus applied loads at the grip create shaft deflections (a-b). Tangential grip loads applied during the early and middle downswing result in clubhead CM deflection towards the shaft CM (black circle); this is manifested as toe-up and lag deflections (c-d). Centripetal grip loads applied in the late downswing result in clubhead CM deflection away from the shaft CM; this is manifested as toe-down and lead (c-d). For equivalent shaft stiffnesses a high kick-point (further from the clubhead) results in a reduced dynamic loft and thus lower trajectory ball flight, the opposite it true for a low kick-point (e) [10].

Majority of the modern iron shafts are drawn from larger diameter steel tubes; successive extrusions create an axially symmetric and hollow geometry that incrementally increases in diameter and decreases in wall thickness from the tip to grip ends. This is followed by heat treatment for desired hardness, roller straightening, acid pickling for oxide removal and surface

finish – for non-stainless steels this includes a nickel-chrome electroplating. Carbon fiber reinforced polymer composite (CFRP) shafts for beginner irons and modern drivers are fabricated by layering laminates around a tapered mandrel. Thin high-temperature plastic is wrapped around the outside to maintain pressure, this arrangement is transferred into an autoclave in the vertical orientation and the epoxy is cured at elevated temperatures and pressures. After cooling the mandrel is removed, thin plastic is stripped off, the surface is sanded smooth and painted for desired cosmetics. Quality control measurements for both steel and CFRP shafts verify that axis linearity and through-length eccentricity are within tolerance. Elastic modulus (E) of a steel shaft can assumed to be an isotropic constant. The effective elastic modulus of a CRFP shaft can be engineered by arranging laminates into specific stacking sequences and orientations relative to the shaft axis. Increasing shaft outer (r_o) and inner (r_i) radii results in an increasing polar, second moment of area from the thicker walled tip to thinner walled grip ends; z denotes position along the shaft axis.

$$I_A(z) = \frac{\pi}{4}(r_o(z)^4 - r_i(z)^4) \tag{7}$$

Measured oscillation frequency (f) of a mass (m) secured at incremental cantilever lengths (L)

$$f = C\sqrt{\frac{EI_A}{mL^3}} \tag{8}$$

along the shaft length is a non-standardized method to empirically validate EI_A stiffness from the tip to butt ends. Stiffness ratings from a given shaft manufacturer: senior, ladies, regular, stiff and extra-stiff are based on the average EI_A stiffness along the shaft length. An optimally fitted shaft will release a greater fraction of stored potential into kinetic energy at impact [11].

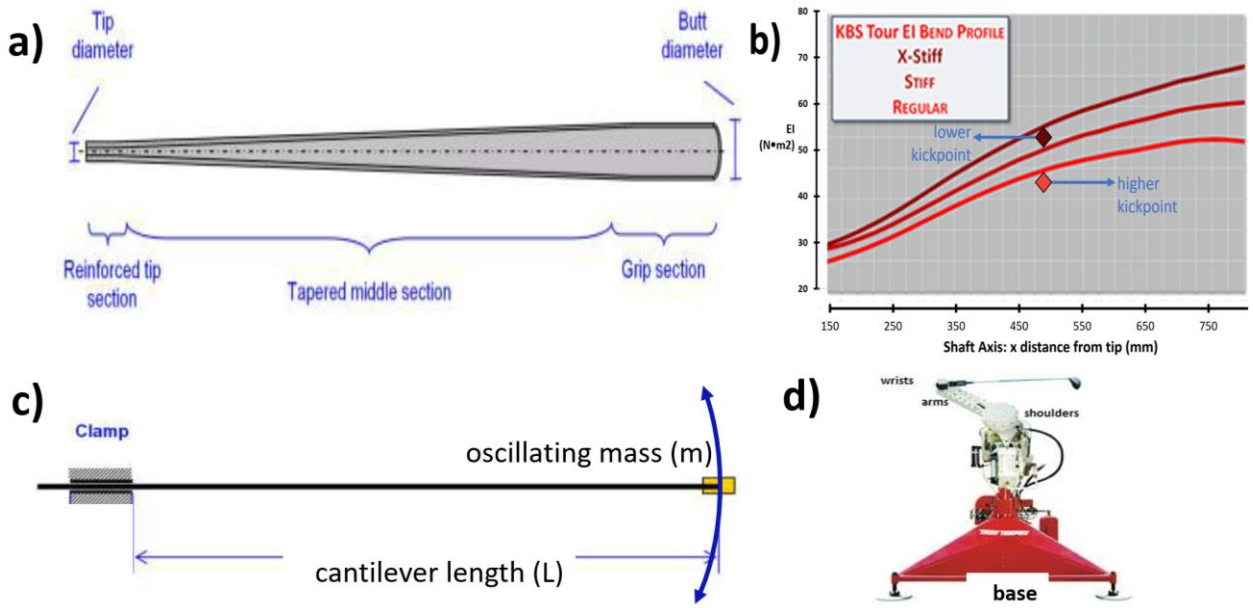

Figure 5: Increasing inner and outer radii of the shaft from the tip to grip sections (a) corresponds to a positive EI_A gradient along the shaft axis (b). More stiff shafts have a greater EI_A gradient corresponding to a kick-point location closer to the tip. Frequency testing (c) is used to empirically validate shaft EI_A profile. Iron Byron is the mechanical tester that verifies how specific downswing kinematics affect dynamic bend profiles of the shaft (d) [11].

VI. Impact Geometry and Ball Flight

D-plane is defined as the positive angle created between the clubhead CM velocity (v_{cm}) and face normal (n) at the clubface center during impact. Shorter shafted, more lofted clubs impact the ball closer to mid-stance before the low-point (Fig 6a). This greater D-plane angle corresponds to a greater tangential velocity component ($v_{cm//}$) imparting a greater angular velocity ($\vec{\omega}_b$) onto the ball (Fig 6b). Longer shafted, less lofted clubs impact the ball closer to lead foot after the low-point (Fig 6c). This reduced D-plane angle corresponds to a greater perpendicular velocity component ($v_{cm\perp}$) imparting a greater compression and velocity (v_b) onto the ball (Fig 6d). Neutral D-plane is defined as parallel to the Z-Y vertical plane, $\vec{\omega}_b$ imparted onto the ball will always be perpendicular to the D-plane. Appropriately modifying address conditions will change downswing clubhead path allowing manipulation of D-plane orientation relative to neutral creating the desired ball flight (Fig 7). Differential boundary layer velocities between the ball top and bottom surfaces (induced by $\vec{\omega}_b$) result in a pressure differential imparting lift onto the ball.

$$\vec{F}_L = \vec{\omega}_b \times \vec{v}_b \quad (9)$$

Frictional forces between the boundary layer and surrounding air exponentially reduce $\vec{\omega}_b$ (and $\vec{F}_L$) during flight, this results in a steeper descent after maximum height resulting in an asymmetrical ball trajectory. The dimpled ball surface reduces Reynold's number. This moves the boundary layer separation point further behind the ball reducing drag force resulting in longer ball trajectories for identical impact conditions. This model for D-plane impact and resulting ball flight is empirically validated using Doppler technology and high-frame rate video capture [12, 13, 14]. The global Cartesian Coordinate system is defined by mutually orthogonal directions: athlete to ball (+x axis), athlete to target (+y-axis), athlete to sky (+z-axis).

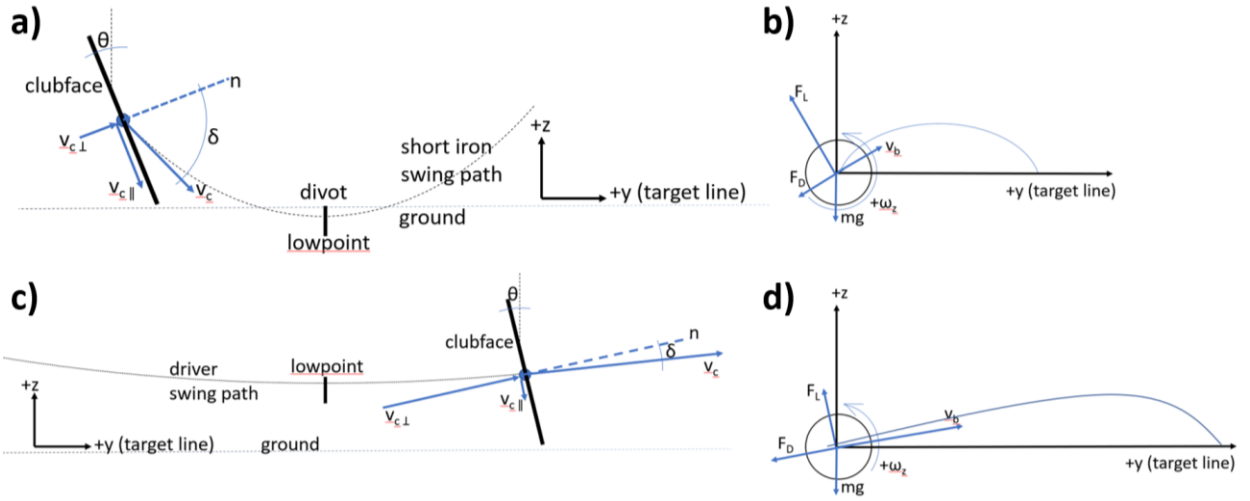

Figure 6: D-plane projection onto the vertical plane YZ plane is described by a +δ angle. Shorter, more lofted clubs (a) impact the ball before the low-point. The greater tangential velocity component ($v_{CM,\parallel}$) imparts a greater ball backspin (+ω_z) for more controlled approach shots near the green (b). Ball elevated on a tee allows the longer, less lofted drivers (c) to create impact after the low-point. The greater velocity component normal to the clubface ($v_{CM,\perp}$) imparts greater ball compression resulting in greater carry distances for shots further from the green (d) [12, 13, 14].

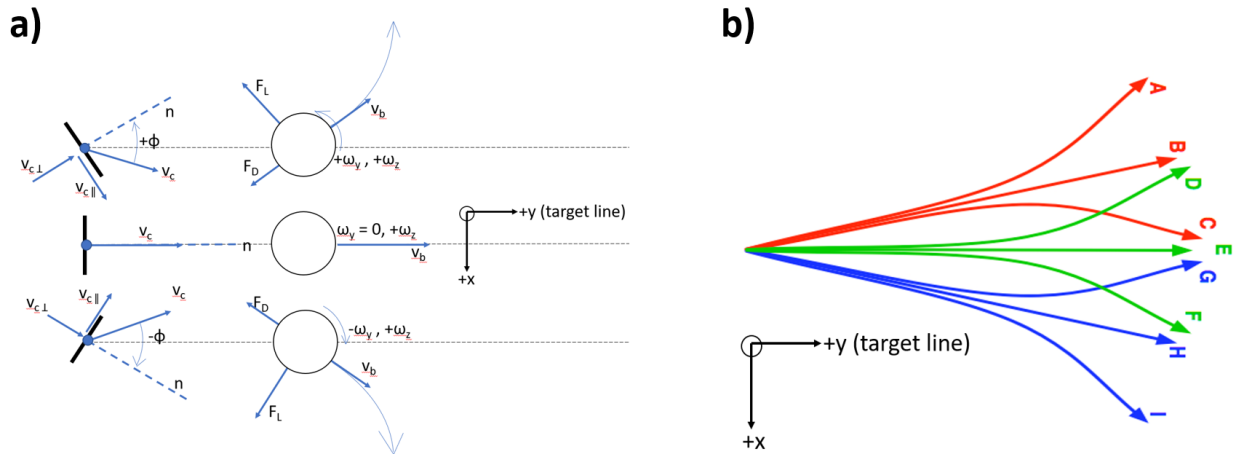

Figure 7: D-plane projection onto the XY horizontal plane (a) is described by a +/-ϕ angle. Manipulation of D-plane orientation relative to neutral creates a variety of ball flights (b). For a right-handed golfer v_{CM} oriented to the right: pull-draw (A), pull (B), pull-fade (C); v_{CM} oriented along target line: straight-draw (D), straight (E), straight-fade (F); and v_{CM} oriented left: push-draw (G), push (H), push-fade (I) [12, 13, 14].

VII. Clubhead Material Mechanics

Ideal clubhead-ball impact occurs at the clubface center coincident with the shortest distance to the clubhead CM. Off-center impacts impart equal but opposite torques onto the clubhead and ball, this imparts unpredictable sidespins resulting in undesired ball flights (Fig 8a). Clubhead design is optimized between a greater $[I]_P$ that mitigates deleterious ball flights due to off-center impacts and a lower $[I]_P$ that permits a more skilled athlete greater control of gamma clubface closure during the late downswing. This permits D-plane manipulation for desired ball flights. Iron clubheads are categorized based on the method of production as either forged (Fig 8b) or investment-cast (Fig 8c) corresponding to lower and greater $[I]_P$ respectively.

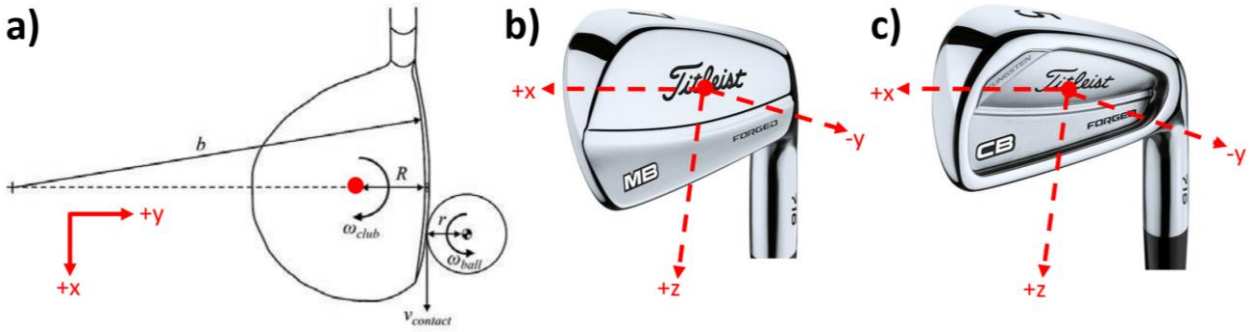

Figure 8: A greater clubhead $[I]_P$ and convex curvature mitigates deleterious ball trajectories created by off-center impacts (a). Anterior oblique views of hot-forged (b) and investment-cast (c) iron clubheads depicting lower and greater $[I]_P$ respectively [16].

Modern driver clubheads are fabricated by welding together three thin convex shapes of steel or titanium alloys creating a hollow shell defined by a crown, face and sole. This construction distributes mass a further distance away from the clubhead CM effectively increasing $[I]_P$ for a given total mass. Driver clubfaces are designed with heel to toe horizontal curvature (bulge), and vertical curvature (roll) imparting initial ball velocity opposite to the curve direction; this further mitigates undesired ball flights for longer trajectories [15, 16, 17]. Current regulations limit clubhead $|[I]_P\hat{k}|$ and displaced volume to 5.9 +/0.1 kg-cm^2 and 460 +/10 cm^3 maximums respectively [1, 2]. A clubface with reduced thickness, greater area and greater material resilience

$$U_r = \frac{\sigma_{YS}^2}{2E} \tag{10}$$

permits greater storage of potential energy thus reducing viscoelastic energy losses within the ball, this enables longer ball trajectories for identical impact geometries. Beta-Titanium alloys are currently the most popular material used for clubhead fabrication due to relatively greater Ur and specific strengths (σ_{YS}/ρ). Bulk metallic glass alloys (BMG) show an even greater potential due to even greater Ur and σ_{YS}/ρ values [Table 1]. However, their low fatigue resistances and propensity to form crystalline grains adjacent to the weld region limits their current use [18, 19, 20].

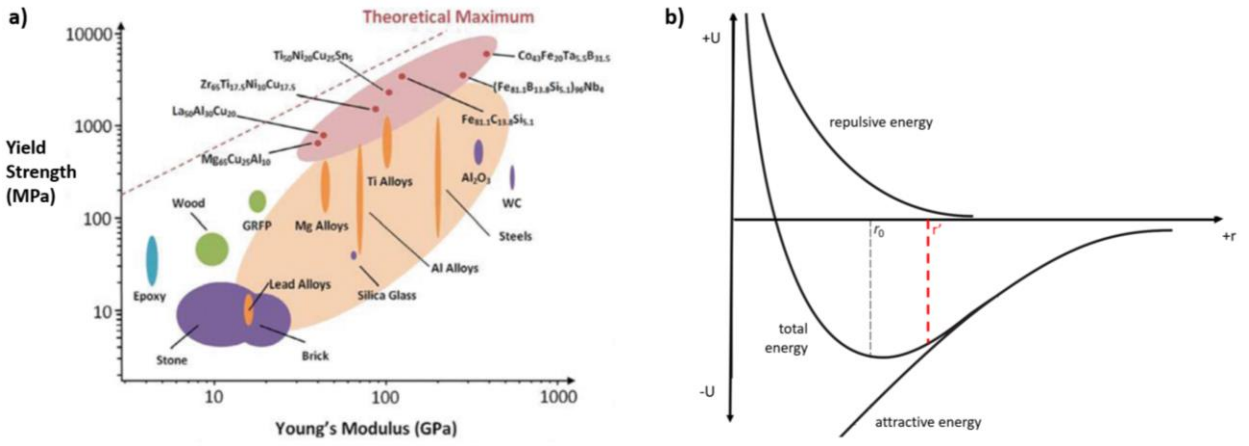

Figure 9: Relative to their corresponding crystalline structures BMG alloys have greater yield strengths and reduced Elastic Moduli (a) and thus greater resilience. Interatomic potential energy (U) is the sum of repulsive and attractive energies (b), BMG have atomic separations (r') greater than equilibrium (r_0) and thus exhibit reduced Elastic Moduli [19, 20].

Table 1: Mechanical and physical properties for golf clubhead and shaft materials. Increased yield strength and decreased E indicate greater material resilience. Only longitudinal mechanical properties shown for anisotropic composites (*) [18, 19, 20].

material	microstructure (crystal)	nominal composition (wt %)	density (g/cc)	E (GPa)	σ_{YS} (MPa)	K_{IC} (Mpa√m)	corrosion resistance
Al 6061	polycrystalline (FCC)	Al - Mg 1.0, Si 0.60, Cr 0.20, Cu 0.28	2.7	69	270	30	Yes
431 Stainless	tempered martensite	Fe - C 0.20max, Mn 1.0max, Cr 16, Ni 1.9	7.8	200	700 - 1000		Yes
17-4PH Stainless	δ-ferrite (BCC) percipitates, martensite matrix	Fe - C 0.07max, Mn 1.0max, Cr 16, Ni 4.0, Cu 4.0, Nb+Ta 0.30	7.8	200	700 - 1200		Yes
C350 Maraging Steel	Ni3(Co, Mo) percipitates, martensite matrix	Fe - 0.03max, Mn 0.10max, Ni 19, Co 12, Mo 4.8, Ti 1.4	8.0	200	1700 - 2300	60	No
Ti-6Al-4V	polycrystalline duplex: α (HCP) + β (BCC)	Ti - Al 6.0, V 4.0	4.5	110	900	30	Yes
Ti-3Al8V6Cr4Mo4Zr	polycrystalline β (BCC)	Ti - Al 3.0, V 8.0, Cr 6.0, Mo 4.0, Zr 4.0	4.8	105	1100 - 1160	65	Yes
ZA27	polycrystalline duplex: α (FCC) + β (HCP)	Zn - Al 27, Mg 0.015, Cu 2.2	5.0	78	200 - 300	18	Yes
Zr - based ternary BMG	amorphous	Zr - Cu 40, Al 10	6.8	88	1860	17	Yes
*CRFP, longitudinal	graphite fiber, epoxy matrix	C, O, N, H					NA
*Persimmon Wood, longitudinal	cellulose fibers (50%), hemicellulose (25%), lignin matrix (25%)	C, O, H	0.8	20	30 - 70	7	NA

In 1998 a conformance criterion was established for clubheads based on the coefficient of restitution (COR) to a 0.83 maximum. This is measured by impacting the clubhead center with a standard Gold Pinnacle ball and determining a ratio of final to initial ball velocities. In 2004 a new pragmatic and informative conformance criteria was established characteristic time (CT) 239+/-

18 μs maximum. This is measured using an instrumented steel ball on a pendulum to strike the clubface center, CT linearly correlates with COR [21].

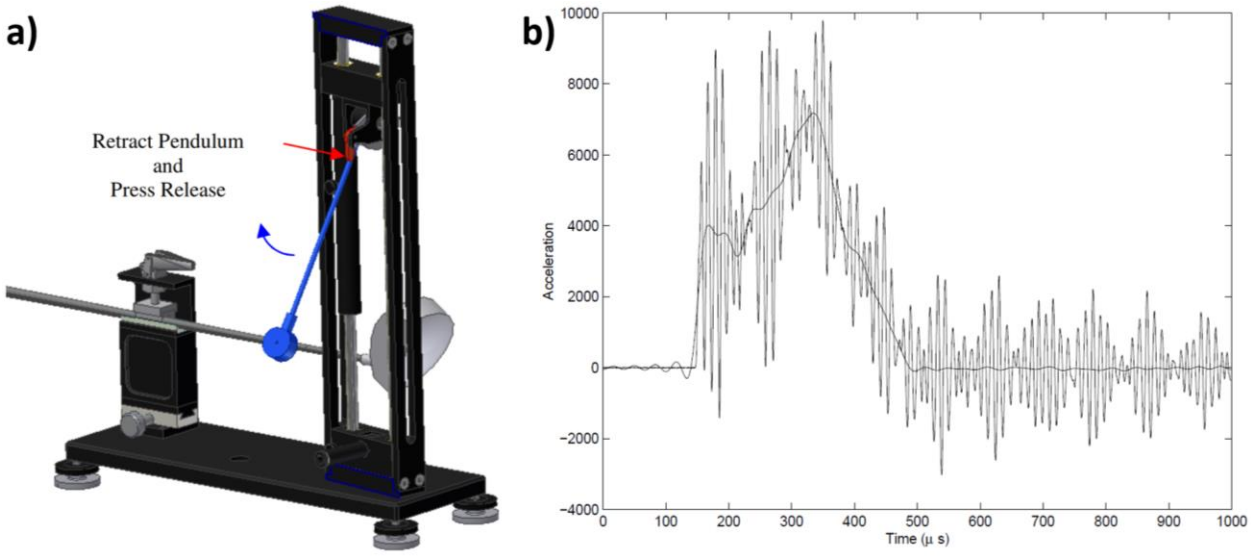

Figure 10: Pendulum testing apparatus is used to measure stiffness of a golf clubhead (a). Clubface center is aligned, grip end is clamped, and pendulum is released. Steel striker is instrumented with a load cell that measures acceleration versus time (b), this signal is filtered to remove high frequency noise so that characteristic time can be determined [21].

VIII. Ball Material Mechanics

Earliest variations of the game were played with smooth balls stitched from natural leathers and stuffed with avian plumage, these were known as *featheries*. In the 1850s this was replaced by a cheaper fabrication from gutta-percha (a type of natural rubber). It was quickly discovered that inscribing grooves on the surface allowed the ball to be hit further distances with more control. Modern golf balls are constructed from 2 to 5 layers, this includes a softer outer cover and harder polybutadiene core [4]. Current regulations dictate that "balls be constructed from primarily elastomeric materials […] exhibit spherical symmetry and pass an initial velocity test." Maximum mass and minimum diameter requirements are regulated to 45.93 g and 42.67 mm [1, 2]. The relationship between stress (σ) and extension ratio (λ) for a hyper-elastic, in-compressible material is described by the Mooney-Rivilin relationship where C_1 and C_2 are empirically determined constants [22].

$$\sigma = 2\left(C_1 + \frac{C_2}{\lambda}\right)\left(\lambda - \frac{1}{\lambda^2}\right) \tag{11}$$

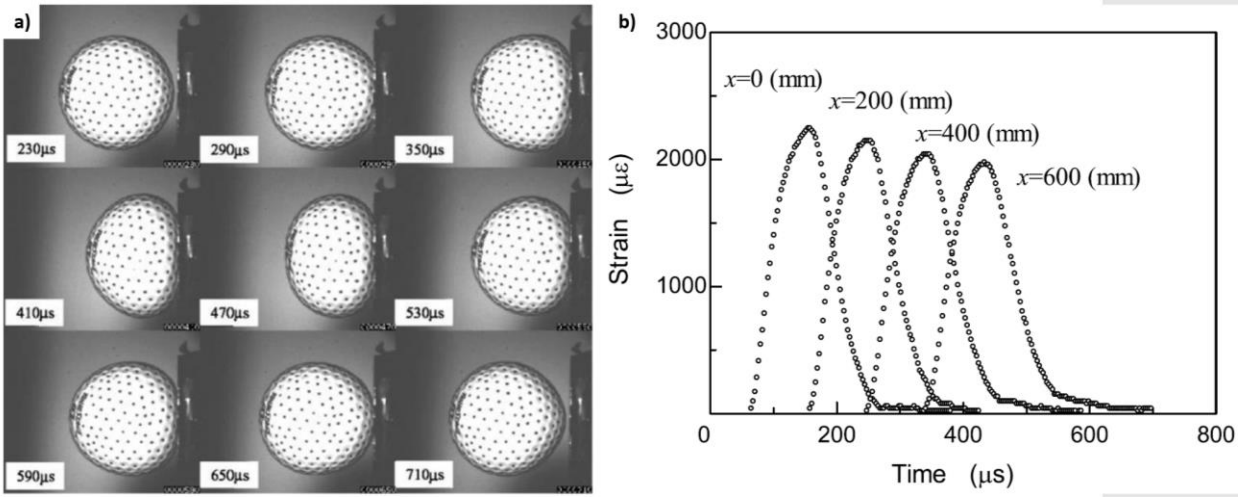

Figure 11: Ball impact on PMMA surface (a) reveals an elastic stress wave propagation resulting in longitudinal compressive and lateral dilation strains [23]. One-dimensional impact test on a PMMA sample reveals longitudinal strain waves that attenuate with increasing distance from the location of impact (x=0) due to internal frictions within the elastomer [24].

IX. Impact Modeling

Impact between the clubface and ball involves forces of several kilo-Newtons and large ball deformations occurring within less than 500 μs thus making direct empirical measurements difficult. Finite element simulations attempt to mechanically model impact conditions using known material properties of the clubhead and ball so that COR and CT can be estimated prior to fabrication of new clubhead designs.

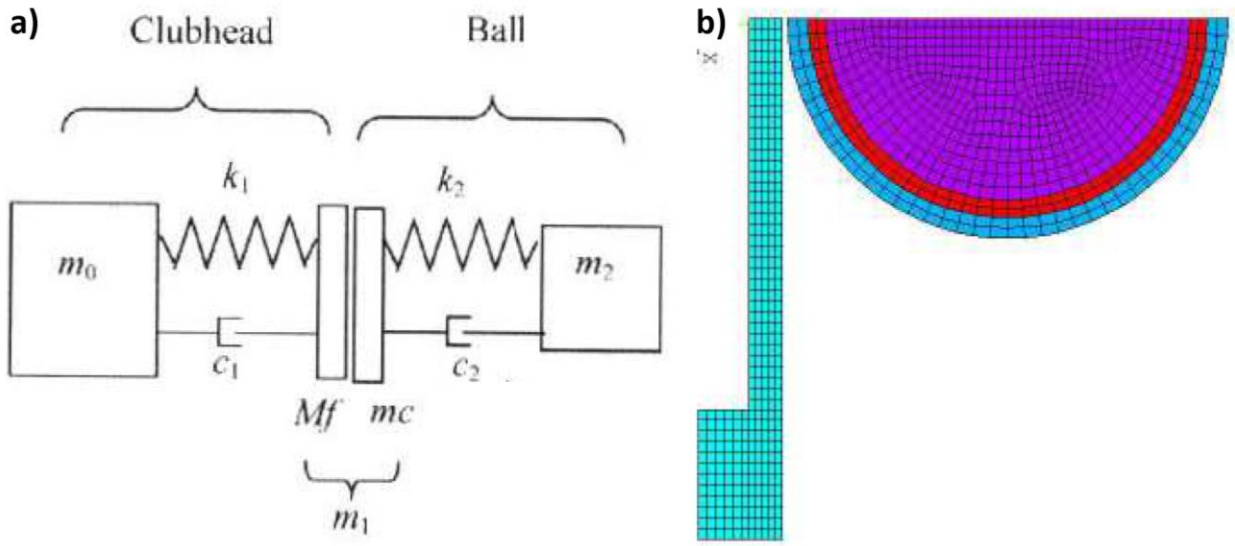

Figure 12: Mechanical model depicting non-rigid clubface (M) impacting a ball. Mesh used in the simulation (b), symmetry is assumed for a normal impact reducing computation costs [25].

X. Conclusion

Golf equipment has experienced significant technological advances coinciding with the advancement of materials science and engineering in the past hundred years. This has made the equipment more affordable and allowed the skilled player to hit the ball greater distances with greater accuracy and precision. However, the average amateur handicap has not improved very much and thus an improved understanding of material behavior during the golf swing combined with a biomechanical assessment of the athlete would assist manufacturers, coaches and players regarding equipment optimization.

References: APA Format

[1] Rules of Golf Modernisation. (n.d.). Retrieved April 17, 2018, from https://www.randa.org/

[2] Rules. (n.d.). Retrieved April 17, 2018, from http://www.usga.org/content/usga/home-page/rules-hub/rulesarticles/rules-fd0eda19.html

[3] *A Review of Driving Distance - 2017*(1.0st ed., pp. 1-24, Rep.). (n.d.). USGA/R&A. DOI: April 16, 2017

[4] Anderson, D. (1999). *The Story of Golf*. New York: Morrow.

[5] Widnall, P. S., Dr. (2008, September). *Lecture L26 - 3D Rigid Body Dynamics: The Inertia Tensor*. Lecture presented at 16.07 Dynamics, Fall 2008 in MIT, Boston, MA. Version 2.1

[6] Solhaug, G. (2015). *U.S. Patent No. US 9022878 B2*. Washington, DC: U.S. Patent and Trademark Office. Method and System for Matching Golf Clubs to Specific User.

[7] Anderson, B. C., Dr. (2007). *Speed Generation in the Golf Swing: An Analysis of Angular Kinematics, Kinetic Energy and Angular Momentum in Player Body Segments*. Master's Thesis, University of Calgary, 2007. Calgary, Alberta: Faculty of Kinesiology and Department of Mechanical Engineering.

[8] Mackenzie, S. J. (2012). Club Position Relative to the Golfers Swing Plane Meaningfully Affects Swing Dynamics. *Sports Biomechanics,11*(2), 149-164. DOI:10.1080/14763141.2011.638388

[9] Jacobs, M., Rudy, M., & Nesbit, S. M., Dr. (2016). *Elements of the Swing: Understanding the New Mechanics of Golf*.

[10] Mackenzie, S. J., & Sprigings, E. J. (2009). Understanding the Mechanisms of Shaft Deflection in the Golf Swing. *Sports Engineering,12*(2), 69-75. doi:10.1007/s12283-010-0034-3

[11] Slater, C. (2011). *The Static and Dynamic Behaviour of Carbon Fibre Composites used in Golf Club Shafts*(Doctoral Dissertation). The University of Birmingham (UK).

[12] T. (2017, April 07). Understanding The D-plane By James Leitz. [Video]. Retrieved April 17, 2018, from https://blog.trackmangolf.com/understanding-d-plane-james-leitz/

[13] Penner, A. R. (2002). The physics of golf. *Reports on Progress in Physics,66*(2), 131-171. doi:10.1088/0034-4885/66/2/202

[14] Kharlamov, A., Chara, Z., & Vlasak, P. (2007). Magnus and Drag Forces Acting on Golf Ball. *Fluid Dynamics,*1-9.

[15] Penner, A. R. (2001). The Physics of Golf: The Convex Face of a Driver. *American Journal of Physics,69*(10), 1073-1081. doi:10.1119/1.1380380

[16] Mcnally, W., Balzerson, D., Wilson, D., & Mcphee, J. (2016). Effect of Clubhead Inertial Properties and Driver Face Geometry on Golf Ball Trajectories. *Procedia Engineering,147*, 407-412. doi:10.1016/j.proeng.2016.06.329

[17] Jenkins, Jenkins, M. L., & NetLibrary, Inc. (2003). 6.8: Head Design Criteria. Materials in Sports Equipment. (pp 146-153). Boca Raton : Cambridge: CRC Press; Woodhead.

[18] Choi, Y., & Hong, S. (2007). Mechanical Properties and Microstructure of Commercial Amorphous Golf Club Heads Made of Zr–Ti–Cu–Ni–Be Bulk Metallic Glass. *Materials Science and Engineering: A,449-451*, 126-129. doi:10.1016/j.msea.2006.02.280

[19] Schnabel, V., Köhler, M., Music, D., Bednarcik, J., Clegg, W. J., Raabe, D., & Schneider, J. M. (2017). Ultra-stiff Metallic Glasses Through Bond Energy Density Design. *Journal of Physics: Condensed Matter,29*(26), 265502. doi:10.1088/1361-648x/aa72cb

[20] Singh, D., Mandal, R., Tiwari, R., & Srivastava, O. (2016). Mechanical Behavior of Zr-Based Metallic Glasses and Their Nanocomposites. *Metallic Glasses - Formation and Properties*. doi:10.5772/64221

[21] *Technical Description of the Pendulum Test* (Publication). (2003). USGA and R&A.

[22] Meyers, M. A., & Chawla, K. K. (2009). *Mechanical Behavior of Materials* (8th ed.). Cambridge: Cambridge University Press.

[23] Tamaogi, T., Sogabe, Y., Wu, Z., & Yokoyama, T. (2017). Identification of Mechanical Models for Golf Ball Materials Using a Viscoelastic Split Hopkinson Pressure Bar. *Journal of Dynamic Behavior of Materials,3*(3), 377-390. doi:10.1007/s40870-017-0115-5

[24] Arakawa, K., Mada, T., Komatsu, H., Shimizu, T., Satou, M., Takehara, K., & Etoh, G. (2007). Dynamic Contact Behavior of a Golf Ball during Oblique Impact: Effect of Friction between the Ball and Target. *Experimental Mechanics,47*(2), 277-282. doi:10.1007/s11340-006-9018-4

[25] Hill, B. P. (2010). *A Finite Element Method Study of Coefficients of Restitution in Golf Driver Clubfaces* (Master's thesis). Rensselaer Polytechnic Institute.